JPE 15-6-16

http://dx.doi.org/10.6113/JPE.2015.15.6.1567
ISSN(Print): 1598-2092 / ISSN(Online): 2093-4718

Harmonic Analysis of the Effects of Inverter Nonlinearity on the Offline Inductance Identification of PMSMs Using High Frequency Signal Injection

Gaolin Wang†, Ying Wang*, Li Ding*, Lei Yang*, Ronggang Ni*, and Dianguo Xu*

†,*School of Electrical Engineering and Automation, Harbin Institute of Technology, Harbin, China

Abstract

Offline inductance identification of a permanent magnet synchronous motor (PMSM) is essential for the design of the closed-loop controller and position observer in sensorless vector controlled drives. On the base of the offline inductance identification method combining direct current (DC) offset and high frequency (HF) voltage injection which is fulfilled at standstill, this paper investigates the inverter nonlinearity effects on the inductance identification while considering harmonics in the induced HF current. The negative effects on d-q axis inductance identifications using HF signal injection are analyzed after self-learning of the inverter nonlinearity characteristics. Then, both the voltage error and the harmonic current can be described. In addition, different cases of voltage error distribution with different injection conditions are classified. The effects of inverter nonlinearities on the offline inductance identification using HF injection are validated on a 2.2 kW interior PMSM drive.

Key words: Estimation error, Harmonic analysis, Inverter nonlinearities, Offline inductance identification, Permanent magnet synchronous motor

I. INTRODUCTION

The permanent magnet synchronous motor (PMSM) has been widely used in industrial applications because of its high efficiency, high power density, good dynamic performance, etc. [1], [2]. Parameter identification is important for performance improvement of the PMSM sensorless vector control which is sensitive to parameter variations, and there have been many studies on the PMSM online parameter identification methodology [3], [4]. In order to meet the emerging demand for modern general-purpose drive applications, more attention should be paid to the offline parameter identification of PMSMs at standstill using only a voltage-source-inverter (VSI) fed drive. The d-q axis inductances of a PMSM obtained from offline identification using high frequency (HF) voltage injection are needed for the proper tuning of closed-loop controllers and the model-based sensorless control scheme [5]-[7]. These critical parameters should be acquired before motor startup. Otherwise the drive system would exhibit poor behavior or even fail to operate. Especially, parameter identification at standstill is essential for applications with load machinery connected, since it is not permissible to make the rotor deviate from its initial position during self-commissioning.

The offline parameter identification methods investigated in [8], [9] require a signal generator that is not suitable for general-purpose drives. This is due to the fact that these signal generator-based test methods need specific instruments. The practical identification strategy using a VSI-fed drive without additional instruments to get accurate d-q axis inductances is important for PMSM control [10]. HF injection is an effective method to estimate inductances by analyzing the relationship between the HF voltage and the induced HF current. However, inverter nonlinearities cause an error of the injected HF signal and influence the accuracy of identification results.

Generally, offline inductance identification strategies using HF injection can be divided into two classes. The first one focuses on HF voltage injection [11], [12]. It is easy to implement and the deterioration of the induced current can reflect the influence of the inverter nonlinearities. The second

Manuscript received Feb. 6, 2015; accepted Jun. 29, 2015
Recommended for publication by Associate Editor Jung-Ik Ha.
†Corresponding Author: wgl818@hit.edu.cn
Tel: +86-8641-3420, Fax: +86-8641-3420
*School of Electrical Engineering and Automation, Harbin Institute of Technology, China

identification method is executed by injecting a HF current signal as the reference of the current-loop using a PI controller. In [13], a proportional resonant (PR) controller was adopted to improve the performance of HF current injection. In this paper, the HF voltage injection based method is adopted.

The main contribution of this paper is that the investigation of the VSI nonlinearities influencing offline inductance identification is proposed by analyzing HF current attenuation and the existence of harmonic components. Additionally, different cases of voltage error distribution with different DC offsets and HF amplitudes are classified. This can effectively describe the negative effects of inverter nonlinearities. All of the signal generation and parameter calculations are performed by a general-purpose PMSM drive. In order to obtain the characteristics of inverter nonlinearities, a self-learning of the inverter nonlinearity parameters using a linear regression algorithm is adopted. The proposed method is validated on a 2.2 kW interior PMSM drive.

II. Proposed Inductance Identification Method

A. Scheme of d-q Axis Inductance Identifications

A VSI-fed drive is adopted to implement offline inductance identification at standstill, and the proposed scheme is shown in Fig. 1. The d-q axis inductance (L_d and L_q) identifications are executed by selecting terminal 1 and 2, respectively. Then, the HF sinusoidal voltage is superposed on the corresponding axis. In addition, a supplementary DC current is injected into the d-axis by using current closed-loop control. This can keep the rotor stay at its initial position and attenuate the influence of inverter nonlinearities.

The HF voltage equation in the d-q axis synchronous rotating frame can be expressed as follows:

$$\begin{cases} u_d = R_s i_d + p\varphi_d - \omega_e \varphi_q \\ u_q = R_s i_q + p\varphi_q + \omega_e \varphi_d \end{cases} \quad (1)$$

where R_s is the stator resistance, p is the differential operator, ω_e is the electrical angular velocity, u_d and u_q are the d-q axis voltages, i_d and i_q are the d-q axis currents, and φ_d and φ_q are the d-q axis flux linkages, respectively. The rotor can be kept at standstill during the identification process. Therefore, (1) can be simplified into:

$$\begin{cases} u_d = R_s i_d + L_d \dfrac{di_d}{dt} \\ u_q = R_s i_q + L_q \dfrac{di_q}{dt} \end{cases}. \quad (2)$$

Thus, L_d and L_q can be estimated according to the HF model as follows:

$$\hat{L}_{d(q)} \approx \frac{\sqrt{\omega_h^2 L_{d(q)}^2 + R_s^2}}{\omega_h} = \frac{U_{inj}}{\omega_h I_{d(q)h}} \quad (3)$$

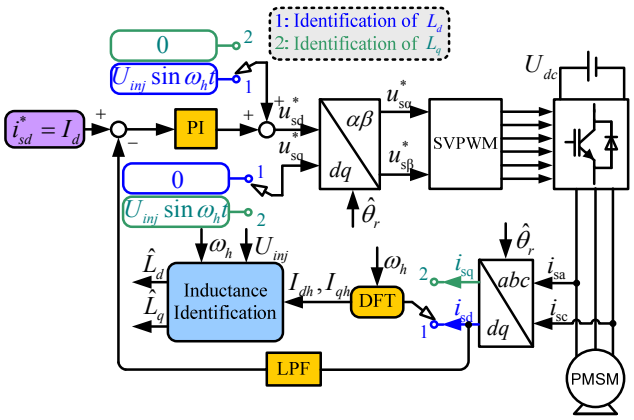

Fig. 1. Proposed scheme of d-q axis inductance identifications.

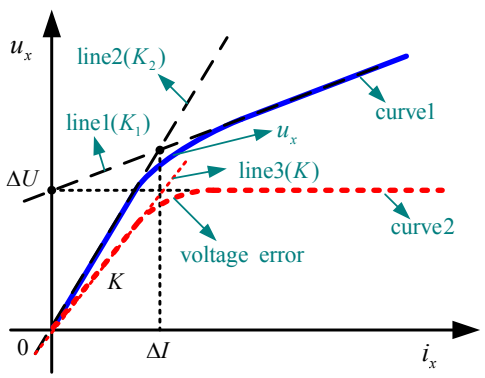

Fig. 2. Relationship between phase voltage and phase current.

where the symbol '^' means the estimated value, U_{inj} and ω_h are the voltage amplitude and the frequency of the injected HF signal, respectively, and I_{dh} and I_{qh} are the amplitudes of the induced d-q axis HF currents.

B. Self-Learning of the Characteristics of Inverter Nonlinearities

Usually, a saturation function is adopted to formulate the equivalent voltage error of inverter nonlinearities without considering the HF injection [14]. Due to the effects of the inverter nonlinearities, the relationship between the phase voltage reference and the phase current is shown in Fig. 2. The phase voltage reference, which increases nonlinearly with a linear increase of the phase current considering the influence of the inverter nonlinearities is indicated as curve 1. Normally, the phase voltage reference is composed with the stator resistance voltage drop and phase voltage error caused by inverter nonlinearities. After subtracting the stator resistance voltage drop, which is proportional to the phase current, the phase voltage error can be illustrated by curve 2. ΔU and ΔI denote the saturation values of the voltage error and the induced current, respectively. They are relevant to the inverter nonlinearities.

As can be seen from Fig. 2, curve 2, which indicates that the voltage error increases linearly with the current in the linear region, performs a resistance behavior. When the

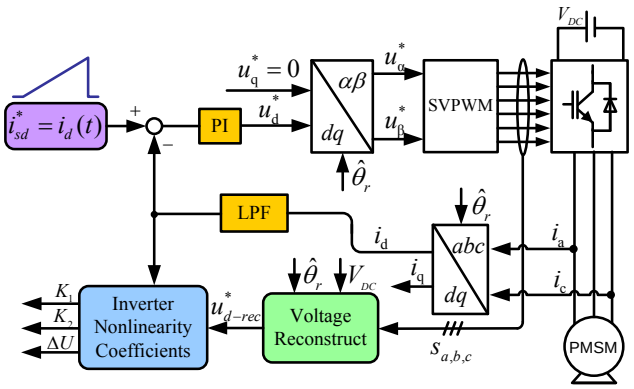

Fig. 3. Self-learning method for acquiring the inverter nonlinearity characteristics at standstill.

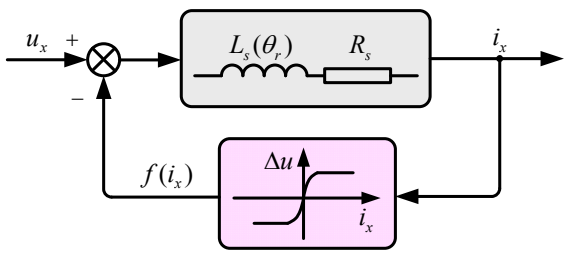

Fig. 4. Nonlinearity model of arbitrary phase *x*.

current exceeds the linear region and enters the saturation region, the voltage error is kept constant. In this period, the gradient of curve 1 which indicates the phase voltage reference decreases. It contains the sum of the stator resistance and the device on-resistance. Additionally, the gradient K_2 in the linear region includes the gradient K_1 in the saturation region. Thus, their relationships can be expressed as follows:

$$\begin{cases} K_1 = R_s + R_{on} \\ K_2 = K_1 + K \end{cases}. \tag{4}$$

In Fig.2, the intercept ΔU of line 1 can be derived by linear regression. Then:

$$\begin{cases} u_x = K_2 i_x, & \text{in linear region} \\ u_x = K_1 i_x + \Delta U, & \text{in saturation region} \end{cases}. \tag{5}$$

Therefore, $K=K_2–K_1$, and the inverter nonlinearity parameters are finally obtained. In order to analyze the harmonic contents in the induced current, K and ΔU should be obtained automatically before the inductance identification by using a self-learning method. The way to get K and ΔU requires keeping the rotor at a standstill.

The self-learning method for acquiring K and ΔU is shown in Fig. 3. Firstly, a linearly increasing current is injected into the d-axis by the closed-loop control. Then the reconstructed phase voltage obtained from the PWM signals $S_{a,b,c}$ and the DC bus voltage U_{dc} contains nonlinearity information. The gradient and intercept of the phase voltage reference used to estimate K and ΔU can be calculated by using the linear regression algorithm. The related formulas used to calculate ΔU and K_1 are shown as follows:

$$\begin{cases} \Delta U = \dfrac{\left(\sum_{j=1}^{n} u_j\right)\left(\sum_{j=1}^{n} i_j^2\right) - \left(\sum_{j=1}^{n} i_j\right)\left(\sum_{j=1}^{n} i_j u_j\right)}{n\left(\sum_{j=1}^{n} i_j^2\right) - \left(\sum_{j=1}^{n} i_j\right)^2} \\ K_1 = \dfrac{n\left(\sum_{j=1}^{n} i_j u_j\right) - \left(\sum_{j=1}^{n} i_j\right)\left(\sum_{j=1}^{n} u_j\right)}{n\left(\sum_{j=1}^{n} i_j^2\right) - \left(\sum_{j=1}^{n} i_j\right)^2} \end{cases}. \tag{6}$$

The calculation of the coefficient K_2 is similar to K_1, and the saturation value of the phase current also can be obtained:

$$\Delta I = \frac{\Delta U}{K_2 - K_1} = \frac{\Delta U}{K}. \tag{7}$$

III. Harmonic Analysis of the Induced HF Phase Current

A. Inverter Nonlinearity Model

Assuming that the HF phase current is $I_1\sin(\omega_h t)$, then the corresponding HF phase voltage can be described as $U_m\cos(\omega_h t\text{-}\varphi)$. The phase inductance is $L_s(\theta_r)$ depending on θ_r. The nonlinearity model of the arbitrary phase x (a, b or c) is shown in Fig. 4.

The model of Fig. 4 can be described as follows:

$$L_x \frac{di_x}{dt} + i_x R_x = u_x - f(i_x) \tag{8}$$

where $f(i_x)$ is the voltage error caused by inverter nonlinearities. It is difficult to obtain a general solution of (8) due to the existence of the nonlinear function $f(i_x)$. Therefore, a practical method is adopted to analyze the HF current harmonics. There are four cases considering the different relationships between the voltage error and the HF current.

B. Partial HF Current Located in the Linear Region - Case 1

The voltage error induced by the harmonic components of the HF current is neglected since its value is very small. In addition, only the fundamental component of the HF current is used for the voltage error analysis. In order to simplify the harmonic analysis, the sigmoid function is approximately replaced by the saturation function.

The first case, which is the most complicated, is that the partial HF current is located in the linear region. The relationship between the voltage error and the HF current is shown in Fig. 5.

From Fig. 6, the voltage error is a clipped sine-wave which can be expressed as:

$$\begin{aligned} \Delta u = &\left[U_0 \sin(\omega_h t) - U_1\right] \cdot u\left[U_0 \sin(\omega_h t) - U_1\right] \\ &- U_0 \sin(\omega_h t) + \Delta U_1 \end{aligned} \tag{9}$$

where ΔU_1 is the DC voltage, $U_0\sin(\omega_h t)$ is the HF sinusoidal

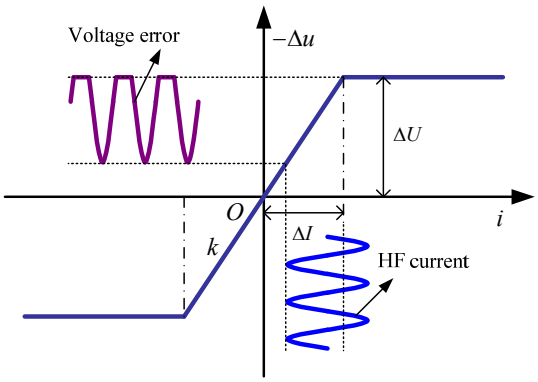

Fig. 5. Relationship between the voltage error and the HF current (case 1).

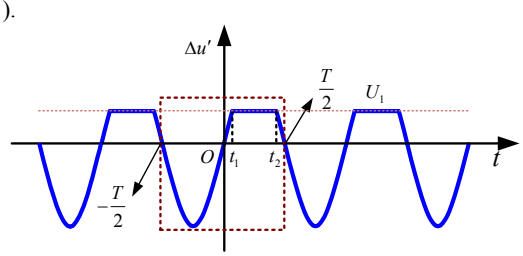

Fig. 6. HF voltage error component in case 1.

voltage, and u(·) is the unit step function. Only the first two terms in (9) induce the HF harmonic current. The first term is the HF fundamental component, and the second term, defined as $\Delta u^{'}$, is solely analyzed into a Fourier series to describe the HF harmonics.

The relationship of the Fourier series in Fig. 6 can be expressed as:

$$\begin{aligned} F(\Delta u^{''}) &= \frac{1}{T}\int_{-T/2}^{T/2}(U_0\sin(\omega_h t)-U_1)\cdot u(U_0\sin(\omega_h t)-U_1)e^{-jn\omega_h t}dt \\ &= \frac{1}{T}\int_{t_1}^{t_2}U_0\sin(\omega_h t)\cdot e^{-jn\omega_h t}dt + \frac{1}{T}\int_{t_1}^{t_2}-U_1\cdot e^{-jn\omega_h t}dt \end{aligned} \tag{10}$$

where the term $\frac{1}{T}\int_{t_1}^{t_2}U_0\sin(\omega_h t)\cdot e^{-jn\omega_h t}dt$ is deduced as follows:

$$\begin{aligned} &\frac{1}{T}\int_{t_1}^{t_2}U_0\sin(\omega_h t)\cdot e^{-jn\omega_h t}dt \\ &= \frac{1}{T}\cdot\frac{1}{-jn\omega_h}\int_{t_1}^{t_2}U_0\sin(\omega_h t)de^{-jn\omega_h t} \\ &= \frac{-1}{jn\omega_h T}[U_1(e^{-jn\omega_h t_2}-e^{-jn\omega_h t_1})] \\ &+ \frac{U_0\cos(\omega_h t_1)}{jn}(e^{-jn\omega_h t_2}+e^{-jn\omega_h t_1}) \\ &+ \frac{\omega_h}{jn}\int_{t_1}^{t_2}U_0\sin(\omega_h t)de^{-jn\omega_h t}] \end{aligned} \tag{11}$$

Define:

$$\begin{cases} \frac{1}{T}\int_{t_1}^{t_2}U_0\sin(\omega_h t)\cdot e^{-jn\omega_h t}dt = M \\ e^{-jn\omega_h t_2}-e^{-jn\omega_h t_1} = A \\ e^{-jn\omega_h t_2}+e^{-jn\omega_h t_1} = B \end{cases}.$$

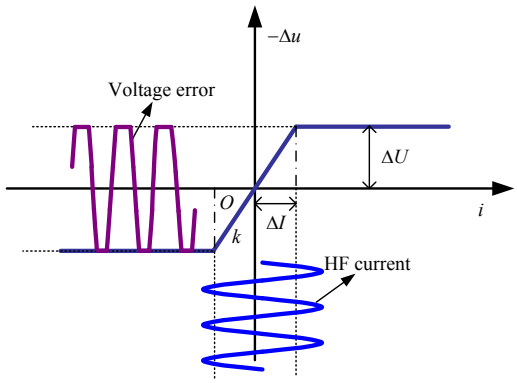

Fig. 7. Relationship between the voltage error and the HF current (case 2).

Then (11) can be simplified into:

$$M = \frac{-U_1}{Tjn\omega_h}A - \frac{U_0\cos(\omega_h t_1)}{Tn^2\omega_h}B + \frac{1}{n^2}M.$$

Thus, M can be obtained:

$$\begin{cases} M = \frac{A[U_1/(Tnj\omega_h)]+B[U_0\cos(\omega_h t_1)/(Tn^2\omega_h)]}{1/n^2-1} & (n\neq 1) \\ M = \frac{U_1\cos(\omega_h t_1)}{2\pi j} & (n=1) \end{cases}. \tag{12}$$

For A and B, there are two situations:

i) when n is even, there is:

$$\begin{cases} A = 2j\sin(n\omega_h t_1) = -2j\sin(n\omega_h t_2) \\ B = 2\cos(n\omega_h t_1) = 2\cos(n\omega_h t_2) \end{cases}. \tag{13}$$

ii) when n is odd, there is:

$$\begin{cases} A = -2\cos(n\omega_h t_1) = 2\cos(n\omega_h t_2) \\ B = -2j\sin(n\omega_h t_1) = -2j\sin(n\omega_h t_2) \end{cases}. \tag{14}$$

As a result, $\frac{1}{T}\int_{t_1}^{t_2}-U_1\cdot e^{-jn\omega_h t}dt = \frac{AU_1}{2\pi jn}$.

This conclusion demonstrates that when $n\neq 1$, there is $F(\Delta u^{''}) = M + \frac{AU_1}{2\pi jn}$. Then, it can be expressed as follows:

$$F(\Delta u^{''}) = \begin{cases} \frac{AU_1+jnBU_0\cos(\omega_h t_1)}{2j\pi(n-n^3)} & (n\neq 1) \\ -\frac{U_1\cos(\omega_h t_1)}{2\pi j} & (n=1) \end{cases}. \tag{15}$$

C. Partial HF Current Located in the Linear Region – Case 2

When the amplitude of the HF current is high enough when compared with the DC component, the maximum and minimum values of the induced current exceed the positive and negative saturation values, respectively. The voltage error is shown in Fig. 7.

From Fig. 7, the voltage error is a clipped sine-wave which can be expressed as:

$$\Delta u = \begin{cases} U_0\sin(\omega_h t)-[U_0\sin(\omega_h t)-U_2]\cdot u[U_2-U_0\sin(\omega_h t)] & t\in[-T/2,0] \\ U_0\sin(\omega_h t)-[U_0\sin(\omega_h t)-U_1]\cdot u[U_0\sin(\omega_h t)-U_1] & t\in[0,T/2] \end{cases}. \tag{16}$$

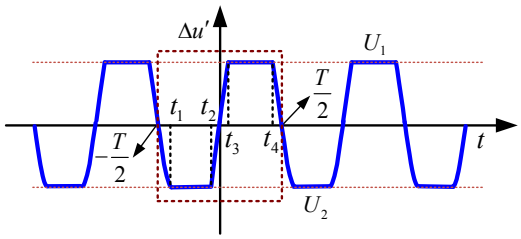

Fig. 8. HF voltage error component in case 2.

According to the same analytical method mentioned in case 1, just analyze the second term of the voltage error which causes the distortion of the induced current in (16). Thus, the clipped sin-wave removing the DC component is shown in Fig.8, where t_1, t_2, t_3, and t_4 are the clipped times, and U_1, and U_2 are the saturation values.

The resolution of the Fourier series of Fig. 8 is:

$$\begin{aligned} F(\Delta u^{''}) &= \frac{1}{T}\left\{\int_{-T/2}^{0}\left[U_0\sin(\omega_h t)-U_2\right]u\left[-U_0\sin(\omega_h t)+U_2\right]e^{-jn\omega_h t}dt\right. \\ &\left.+\int_{0}^{T/2}\left[U_0\sin(\omega_h t)-U_1\right]u\left[U_0\sin(\omega_h t)-U_1\right]\cdot e^{-jn\omega_h t}dt\right\} \\ &= \frac{1}{T}\int_{t_1}^{t_2}U_0\sin(\omega_h t)\cdot e^{-jn\omega_h t}dt-\frac{1}{T}\int_{t_1}^{t_2}U_2\cdot e^{-jn\omega_h t}dt \\ &+\frac{1}{T}\int_{t_3}^{t_4}U_0\sin(\omega_h t)\cdot e^{-jn\omega_h t}dt-\frac{1}{T}\int_{t_3}^{t_4}U_1\cdot e^{-jn\omega_h t}dt \end{aligned} \quad (17)$$

According to the same analysis method introduced in case 1, the result is;

i) when $n\neq 1$, (17) can be expressed into:

$$F(\Delta u^{''}) = \frac{AU_1+jnBU_0\cos(\omega_h t_1)+CU_2+jnDU_0\cos(\omega_h t_3)}{2j\pi(n-n^3)} \quad (18)$$

where A, B, C, and D can be expressed as:

$$\begin{cases} A=2j\sin(n\omega_h t_1) \\ B=2\cos(n\omega_h t_1) \\ C=2j\sin(n\omega_h t_3) \\ D=2\cos(n\omega_h t_3) \end{cases} n \text{ is even}, \quad \begin{cases} A=-2\cos(n\omega_h t_1) \\ B=-2j\sin(n\omega_h t_1) \\ C=-2\cos(n\omega_h t_3) \\ D=-2j\sin(n\omega_h t_3) \end{cases} n \text{ is odd} \quad (19)$$

ii) when n=1, (17) can be expressed into:

$$F(\Delta u^{''}) = -\frac{U_1\cos(\omega_h t_1)+U_2\cos(\omega_h t_3)}{2\pi j}. \quad (20)$$

D. Whole HF Current Located in the Linear Region – Case 3

Similarly, in Fig. 8, when the whole HF current is located in the linear region, the induced voltage error has the same phase as the HF current shown in Fig. 9. In this case, the voltage error only contains the sinusoidal component without other harmonics and can be expressed as Δu=-U_0*sin*(ω_h-*t*)+ΔU_1. The equivalent HF resistance reaches its maximum that is equal to the gradient of the linear region.

E. Whole HF Current Located in the Saturation Region – Case 4

When the DC current component is high enough, the HF current will be far away from the linear region and the voltage error is constant as shown in Fig. 10. The equivalent HF resistance reaches its minimum and is equal to zero. Thus, the voltage error does not affect the identification result in this case.

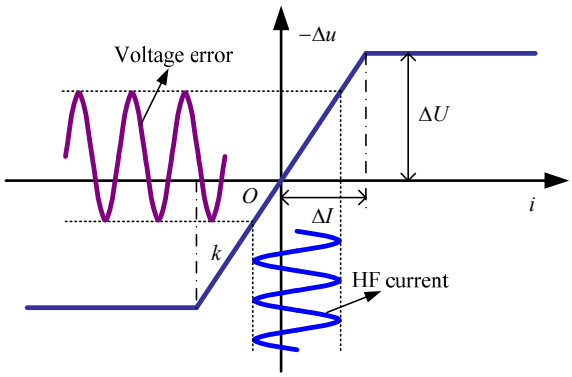

Fig. 9. Relationship between the voltage error and the HF current (case 3).

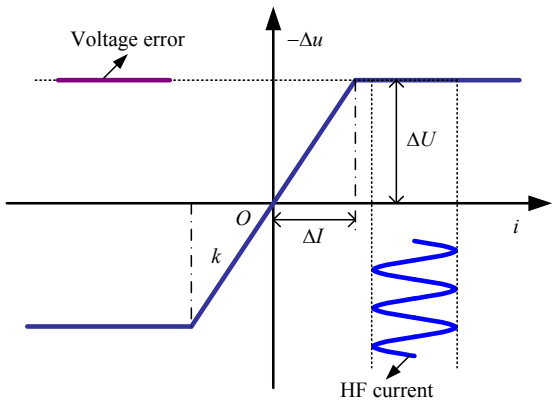

Fig. 10. Relationship between the voltage error and the HF current (case 4).

According to the inverter nonlinearity parameters, which are obtained by the self-learning method introduced in Part II, a two-dimensional region can be established based on the HF amplitude and DC offset of the induced current. Fig. 11 shows the regions of the four cases in the first quadrant, where the current saturation value ΔI is 0.1pu (the current base value is selected as 7.9A), and the voltage error saturation value ΔU is 0.044pu (the voltage base value is selected as 311V).

Define the HF amplitude and DC offset of the induced current as X and Y, respectively. When X and Y meet -0.1<-X+Y<0.1 and -0.1<X+Y<0.1, they belong to case 3. When X and Y meet –X+Y>0.1, they belong to case 4. In these two cases, the voltage error only contains the sinusoidal component without other harmonics. When X and Y meet the conditions -0.1<-X+Y<0.1 and X+Y>0.1, they belong to case 1. Thus, U_0=0.4X and U_1=0.04-0.4Y. When X and Y meet the conditions -X+Y<-0.1 and X+Y>0.1, they belongs to case 2. Thus, U_0=0.4X, U_1=0.04-0.4Y, and U_2=-0.04-0.4Y.

After analyzing the distribution of the four cases in the two-dimensional region, the 2nd and 3rd harmonics are

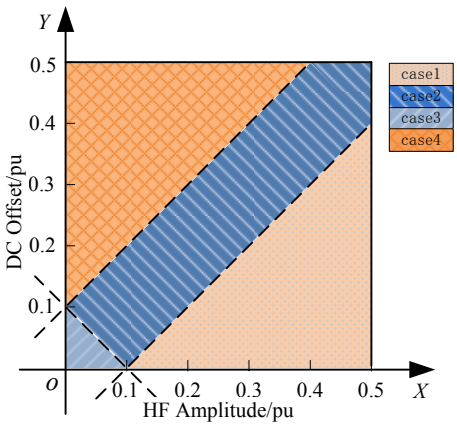

Fig. 11. Different effects of the inverter nonlinearities described by two-dimensional region with four cases.

selected to be analyzed because the amplitudes of the high-order harmonics are very small and can be neglected. According to the harmonic analysis above, the amplitudes of the 2nd and 3rd harmonics, which are represented by A_2 and A_3, can be obtained:

$$A_2=\begin{cases}\dfrac{2}{3\pi}U_0\cdot\left(\cos\omega_h t_1\right)^3, & case1\\ \dfrac{2}{3\pi}\left[U_0\left(\cos\omega_h t_1\right)^3-U_0\cdot\left(\cos\omega_h t_3\right)^3\right], & case2\\ 0, & case3\\ 0, & case4\end{cases}, \quad (21)$$

$$A_3=\begin{cases}\dfrac{2}{3\pi}U_1\cdot\left(\cos\omega_h t_1\right)^3, & case1\\ \dfrac{2}{3\pi}\left[U_1\cdot\left(\cos\omega_h t_1\right)^3-U_2\cdot\left(\cos\omega_h t_3\right)^3\right], & case2\\ 0, & case3\\ 0, & case4\end{cases}. \quad (22)$$

F. Inverter Nonlinearity Effects on Offline Inductance Identification

According to the above analysis, the inverter nonlinearities cause voltage errors during the offline inductance identification process. The actual voltage drop of the d-q inductances and stator resistance is $U_{inj}\sin(\omega_h t)-\Delta u$. Therefore, the induced current $I_{d(q)}$can be expressed as follows:

$$I_{d(q)}=\frac{u_{inj}\sin(\omega_h t)-\Delta u}{\omega_h L_{d(q)}} \quad (23)$$

According to (3), the estimated values of the d-q inductances are larger than the theoretical values due to the effects of inverter nonlinearities. In addition, the relationship between the estimated and theoretical values can be obtained:

$$\hat{L}_{d(q)}=\frac{U_{inj}}{\left|U_{inj}\sin(\omega_h t)-\Delta u\right|}L_{d(q)} \quad (24)$$

where $|U_{inj}\sin(\omega_h t)-\Delta u|$ is the fundamental component amplitude of $U_{inj}\sin(\omega_h t)-\Delta u$, and $\hat{L}_{d(q)}$ and $L_{d(q)}$ are the estimated and theoretical values of the d-q inductances, respectively.

Fig. 12. Experimental platform of 2.2kW IPMSM.

The voltage errors caused by inverter nonlinearities vary with the signal injection condition. There are inevitable estimation errors in case 1, case 2 and case 3 due to the fundamental voltage error. In case 4, the fundamental voltage error is zero and the DC voltage error does not influence the inductance estimation.

IV. Experimental Results

The analysis of the inductance identification algorithm has been validated in a 2.2kW interior PMSM (IPMSM) drive as shown in Fig. 12. The rated parameters of the IPMSM are listed as follows: 380V, 5.6A, 50Hz, 21Nm, and 1000r/min. An intelligent power module FP25R12KT4 is used. A STM32F103 ARM is adopted to execute the whole identification algorithm. The PWM frequency is 6kHz, and the dead time is 3.2μs. The frequency of the injected HF voltage signal is 300Hz. The current reference increases linearly with 0.03pu/s during the estimation of the inverter nonlinearity parameters. A 12-bit absolute encoder is installed to obtain the actual position. This is used solely for showing the electrical angle of the rotor during the identification process.

The waveform of the whole identification process is shown in Fig. 13. The a-phase current and the estimated L_d and L_q are given. The rotor position is obtained by the initial position identification method. This method can realize the identification process at standstill. The supplementary d-axis DC current is 0.1pu. The injected HF voltage increases gradually to avoid overcurrent and to guarantee signal intensity. The d-q axis inductances converge to stable values, 32.4mH (the theoretical value of L_d is 31.6mH) and 65.2mH (the theoretical value of L_q is 62.8mH), respectively.

Fig.14 shows the actual and estimated rotor position waveforms during the inductance identification process with different initial rotor positions. Firstly, the HF voltage signal is injected to obtain the initial position. Then, a pulse signal is

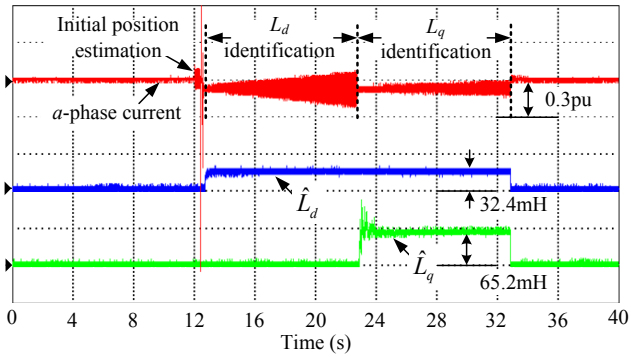

Fig. 13. Experimental waveforms of the d-q axis inductance identification.

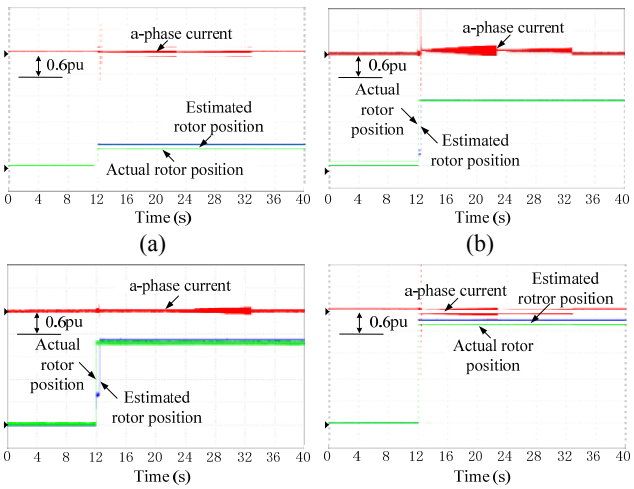

Fig. 14. Experimental waveforms of the actual and estimated rotor position during the inductance identification process. (a) 46º, (b) 200 º, (c) 257 º, and (d) 328 º.

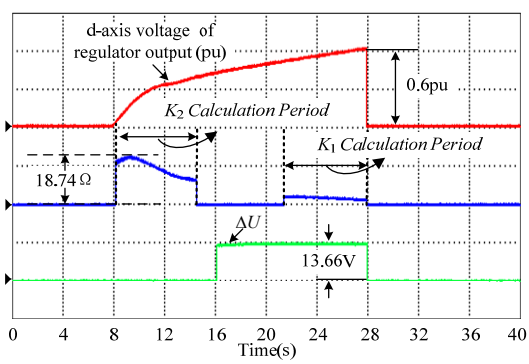

Fig. 15. Experimental waveforms of the self-learning process.

injected to detect the polarity. After acquiring the initial rotor position, the inductance identification process can be started. The actual rotor positions in Fig. 14(a), (b), (c), and (d) are 46º, 200º, 257º, and 328º, respectively, while the estimated rotor positions are 50º, 203º, 262º and 334º, respectively. From Fig. 14, the position stays constant during the identification process. The results indicate that the proposed inductance identification method can be operated at a standstill no matter what the initial rotor position is.

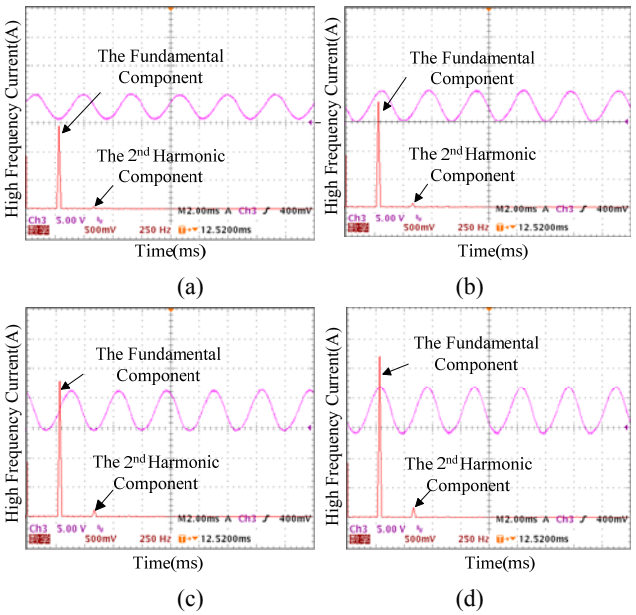

Fig. 16. Harmonic analysis of the induced current considering the effects of the inverter nonlinearities with different HF amplitudes, (a) 0.15pu, (b) 0.2pu, (c) 0.25pu, and (d) 0.3pu.

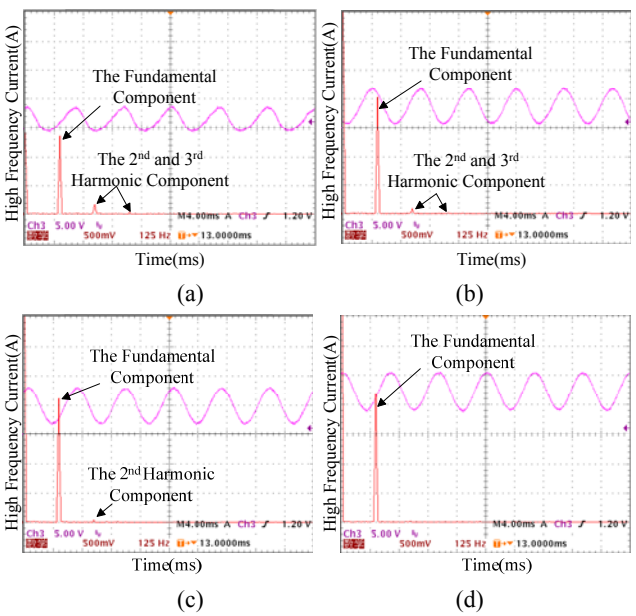

Fig. 17. Harmonic analysis of the induced current considering the effects of the inverter nonlinearities with different DC offsets, (a) 0.05pu, (b) 0.15pu, (c) 0.2pu, and (d) 0.3pu.

Fig. 15 shows the experimental waveforms of the self-learning process for the inverter nonlinearity parameters. From top to bottom, the d-axis voltage reference of the current regulator output, the estimated inverter nonlinearity gradient parameter, and the estimated saturation value of the voltage are given. According to (4), the inverter nonlinearity gradient K is equal to 15.8Ω. The saturation value of the voltage error is 13.66V.

Fig. 16 shows the harmonic analysis of the induced current with different HF amplitudes when the DC offset is 0.12pu.

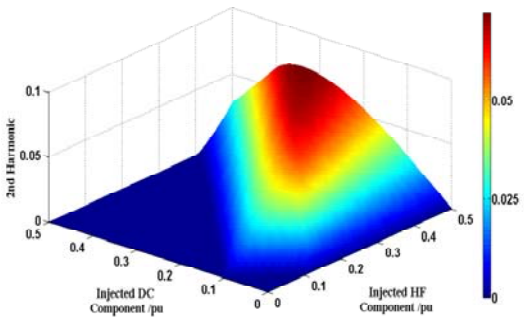

(a)

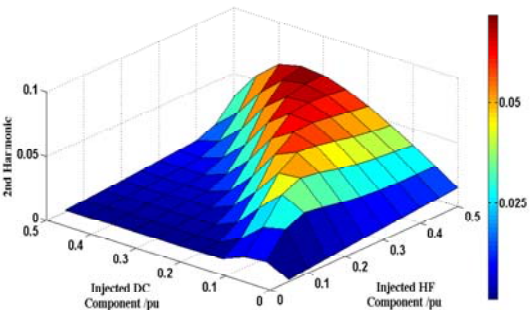

(b)

Fig. 18. Analysis of the 2nd harmonic caused by voltage error with different DC offsets and HF amplitudes, (a) the theoretical result, (b) the experimental result.

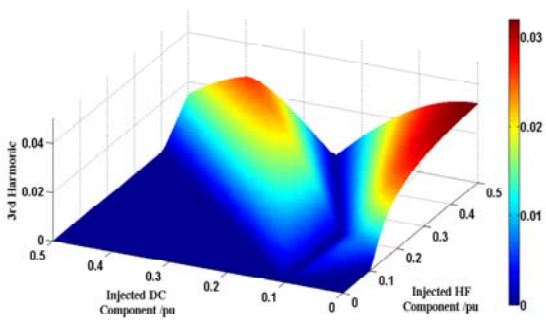

(a)

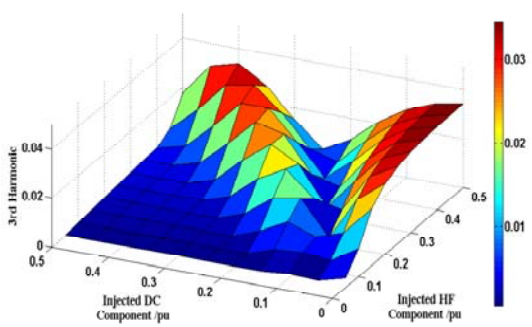

(b)

Fig. 19. Analysis of the 3rd harmonic caused by voltage error with different DC offsets and HF amplitudes, (a) the theoretical result, (b) the experimental result.

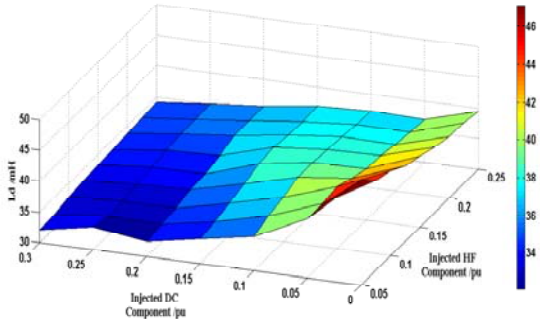

Fig. 20. The experimental results of L_d estimation under different injection conditions.

From these results, the amplitude of the 2nd harmonic component increases as the HF amplitude becomes larger.

Fig. 17 shows the harmonic analysis of the induced current with different DC offsets when the HF amplitude is 0.1pu. It can be seen that the amplitude of the 2nd harmonic component decreases as the DC offset becomes larger.

Fig. 18 and Fig. 19 show the theoretical and experimental results of the 2nd and 3rd harmonics of the induced current caused by voltage errors with different DC offsets and HF amplitudes. The experimental results closely match the theoretical results.

The experimental result of the L_d identification is given to verify the effectiveness of the proposed analysis. Fig. 20 shows the estimated value of L_d under different injection conditions. It can be seen from these results that with the increasing of the DC current component, the estimated value of L_d is more accurate. When the injected DC component and the HF component are relatively small as case 3 shows, the maximum estimation error reaches 44.9%, while the maximum estimation error is reduced to 4.6% in case 4 when the DC component is high enough.

V. Conclusion

The harmonic analysis method of inverter nonlinearity effects on offline inductance identification with a DC offset and high frequency voltage injection for PMSMs at standstill using a VSI-fed drive was proposed. The parameters of the inverter nonlinearities can be obtained by the self-learning method. Then the current harmonic induced by inverter nonlinearities was analyzed in four different cases with different injection conditions. The rotor can be kept at the initial position during the inductance identification and inverter nonlinearity estimation processes. The proposed offline inductance identification can be applied in general-purpose drives for PMSM sensorless control. According to the characteristics of the inverter nonlinearities, the harmonic analysis can be accomplished. The experimental results match the theoretical results closely.

ACKNOWLEDGMENT

The research work was supported by the Research Fund for the National Science Foundation of China (51207030, 51522701), grants from the Power Electronics Science and Education Development Program of Delta Environmental & Educational Foundation (DREK2015002), and the Fundamental Research Funds for the Central Universities (HIT.BRETIII.201407).

REFERENCES

[1] Y. S. Jung and M. G. Kim, "Sliding mode observer for sensorless control of IPMSM," *Journal of Power Electronics*, Vol. 9, No. 1, pp. 117-123, Jan. 2009.

[2] G. Wang, R. Yang, and D. Xu, "DSP-based control of sensorless IPMSM drives for wide-speed-range operation," *IEEE Trans. Ind. Electron*., Vol. 60, No. 2, pp. 720-727, Feb. 2013.

[3] M. A. Hamida, J. D. Leon, A. Glumineau, and R. Boisliveau, "An adaptive interconnected observer for sensorless control of PM synchronous motors with online parameter identification," *IEEE Trans. Ind. Electron*., Vol. 60, No.2, pp. 739-748, Feb. 2013.

[4] K. Liu, Z. Q. Zhu, Q. Zhang, and J. Zhang, "Influence of nonideal voltage measurement on parameter estimation in permanent- magnet synchronous machines," *IEEE Trans. Ind. Electron*., Vol. 59, No.6, pp. 2438-2447, Jun. 2012.

[5] Z. Chen, X. Deng, K. Huang, W. Zhen, and Lei Wang, "Sensorless control of wound rotor synchronous machines based on high-frequency signal injection into the stator windings," *Journal of Power Electronics*, Vol. 13, No. 4, pp. 669-677, Jul. 2013.

[6] A. Boglietti, A. Cavagnino, and M. Lazzari, "Experimental high- frequency parameter identification of AC electrical motors," *IEEE Trans. Ind. Appl.*, Vol. 43, No.1, pp. 23-29, Jan./Feb. 2007.

[7] F. Cupertino, G. Pellegrino, P. Giangrande, and L. Salvatore, "Sensorless position control of permanent-magnet motors with pulsating current injection and compensation of motor end effects," *IEEE Trans. Ind. Appl.*, Vol. 47, No. 3, pp. 1371-1379, May/Jun. 2011.

[8] R. Dutta and M. F. Rahman, "A comparative analysis of two test methods of measuring d- and q-axes inductances of interior permanent- magnet machine," *IEEE Trans. Magn.*, Vol. 42, No. 11, pp. 3712-3718, Nov. 2006.

[9] K. M. Rahman and S. Hiti, "Identification of machine parameters of a synchronous motor," *IEEE Trans. Ind. Appl*., Vol. 41, No. 2, pp. 557-565, Mar./Apr. 2005.

[10] M. A. Arjona, M. Cisneros-González, and C. Hernández, "Parameter estimation of a synchronous generator using a sine cardinal perturbation and mixed stochastic-deterministic algorithms," *IEEE Trans. Ind. Electron*., Vol. 57, No. 1, pp. 430-439, Jan. 2010.

[11] Y. S. Je and J. Y. Lee, "Parameter identification of an induction motor drive with magnetic saturation for electric vehicle," *Journal of Power Electronics*, Vol.11, No. 4, pp. 418-423, Jul. 2011.

[12] J. M. Guerrero, M. Leetmaa, F. Briz, A. Zamarrón, and R. D. Lorenz, "Inverter nonlinearity effects in high-frequency signal- injection-based sensorless control methods," *IEEE Trans. Ind. Appl.*, Vol. 41, No. 2, pp. 618-626, Mar./Apr. 2005.

[13] S. A. Odhano, P. Giangrande, R. I. Bojoi, and Chris Gerada, "Self-commissioning of Interior Permanent-Magnet Synchronous Motor Drives With High-Frequency Current Injection," *IEEE Trans. Ind. Electron*., Vol. 50, No. 50, pp. 3295-3303, Sep. 2014.

[14] Y. Park and S. K. Sul, "A novel method utilizing trapezoidal voltage to compensate for inverter nonlinearity," *IEEE Trans. Power Electron*., Vol. 27, No. 12, pp. 4837-4846, Jun. 2012.

Gaolin Wang (M'13) received his B.S., M.S. and Ph.D. degrees in Electrical Engineering from the Harbin Institute of Technology, Harbin, China, in 2002, 2004 and 2008, respectively. In 2009, he became a Lecturer in the Department of Electrical Engineering, Harbin Institute of Technology, where he has been a Full Professor of Electrical Engineering, since 2014. From 2009 to 2012, he was a Postdoctoral Fellow in the Shanghai Step Electric Corporation, Shanghai, China, where he was involved in traction machine control for direct-drive elevators. He has authored more than 50 technical papers published in journals and conference proceedings. He is the holder of 10 Chinese patents. His current research interests include permanent magnet synchronous motor drives, high performance direct-drives for traction systems, position sensorless control of AC motors, and digital control of power converters.

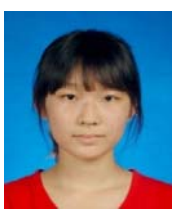

Ying Wang received her B.S. degree in Electrical Engineering from the Harbin Institute of Technology, Harbin, China, in 2014, where he is presently working toward her M.S. degree in Power Electronics and Electrical Drives in the School of Electrical Engineering and Automation. Her current research interests include the position sensorless control of IPMSMs.

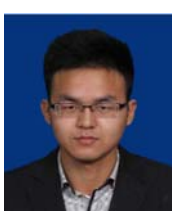

Li Ding received his B.S. degree in Electrical Engineering from Shanghai University, Shanghai, China, in 2013. He is presently working toward his M.S. degree in Power Electronics and Electrical Drives in the School of Electrical Engineering and Automation, Harbin Institute of Technology, Harbin, China. His current research interests include permanent magnet synchronous motor drives and position sensorless control.

Lei Yang received his B.S. degree in Electrical Engineering from the Harbin Institute of Technology, Harbin, China, in 2015, where he is presently working toward his M.S. degree in Power Electronics and Electrical Drives in the School of Electrical Engineering and Automation. His current research interest include permanent magnet synchronous motor drives.

Ronggang Ni received his B.S. and M.S. degrees in Electrical Engineering from the Harbin Institute of Technology, Harbin, China, in 2010 and 2012, respectively. He is presently working toward his Ph.D. degree in Power Electronics and Electrical Drives in the School of Electrical Engineering and Automation, Harbin Institute of Technology. His current research interests include the optimal design and control of permanent magnet synchronous motors.

Dianguo Xu (M'97, SM'12) received his B.S. degree in Control Engineering from the Harbin Engineering University, Harbin, China, in 1982, and his M.S. and Ph.D. degrees in Electrical Engineering from the Harbin Institute of Technology (HIT), Harbin, China, in 1984 and 1989 respectively. In 1984, he became an Assistant Professor in the Department of Electrical Engineering, HIT. Since 1994, he has been a Professor in the Department of Electrical Engineering, HIT. From 2000 to 2010, he was the Dean of the School of Electrical Engineering and Automation, HIT, and from 2010 to 2014, he was the Assistant President of HIT. He is presently the Vice President of HIT. He has published over 600 technical papers. His current research interests include renewable energy generation technology, sensorless vector controlled motor drives, and high performance PMSM servo systems. Dr. Xu is an Associate Editor of the IEEE Transactions on Industrial Electronics and the IEEE Journal of Emerging and Selected Topics in Power Electronics.